OPERA: An Optical Packet Experimental Routing Architecture with Label Swapping Capability

A. Carena, M. D. Vaughn, R. Gaudino, M. Shell, and Daniel J. Blumenthal, *Senior Member, IEEE*

***Abstract*— This paper describes experimental and simulation results of the optical packet experimental routing architecture (OPERA) project. The OPERA network is based on a novel optical network interface router design that is optically regenerative and supports optical internet protocol related functions including label swapping, packet routing and forwarding operations and wavelength reuse. Routing is based on subcarrier multiplexed header addressing, packet-rate wavelength conversion, and arrayed waveguide router technology. The routers are cascadable and use a unique double stage wavelength converter that supports header regeneration/replacement and maintains the payload extinction ratio. This approach overcomes dispersion limitations normally encountered using double sideband subcarrier multiplexing across a network. A discrete time simulation of the physical transport in an 8-hop network is reported. Multihop routing is experimentally demonstrated between two all-optical nodes and three input–output (I–O) ports of a waveguide grating array router. Packet-rate subcarrier header processing and wavelength conversion between six wavelengths is shown with high signal-to-noise ratio (SNR) of recovered payload and headers at each hop.**

I. Introduction

MULTIHOP wavelength-routed all-optical packet networks have the potential to realize high-throughput, scalable, data-rate, and format independent routing for future packet-based communications applications. Optical routers that process headers and forward packets to a local host or to another router are a critical network element and have been demonstrated to varying degrees [1], [2]. Important features of future routers are the ability to replace packet headers in real time for label swapping [3], perform packet-rate wavelength conversion, and regenerate payload and header optical signals to allow cascading of many nodes. Label swapping is an important technique that has promise to allow simple, high-performance packet forwarding while decoupling the packet routing and forwarding operations to support multiple routing services [3]. Experimental demonstrations of optical header replacement with wavelength conversion [4], [5], and optical regeneration with wavelength conversion [6] have been previously reported.

In this paper, we describe an optical packet experimental routing architecture (OPERA) and present results of a multinode discrete time simulation and multinode experimental demonstration. OPERA supports wavelength reuse, packet level routing and forwarding and label swapping capabilities. The network is divided into subnets that support routing between local users and other subnets via optical network interface routers (ONIR's) and optical arrayed waveguide grating router (AWGR) technology [7]. The ONIR's support header recovery, packet forwarding computation, packet-rate wavelength conversion, header replacement and payload signal regeneration.

An eight hop network is analyzed using a discrete time physical propagation simulator and we present what we believe to be the first experimental demonstration of a multinode WDM multihop packet network interconnected with an AWGR. Each node has the full functionality to route packets with subcarrier multiplexed headers and to perform fast wavelength translation between four wavelengths and space switching between a local host and an 8×8 AWGR. Packets consist of 2.5 Gb/s payloads and 100 Mb/s headers multiplexed on a 3 GHz subcarrier.

II. Network Architecture

The OPERA network is designed to route packets between users across multiple subnets as shown in Fig. 1. Each subnet connects M users via ONIR's and provides connections to $N-M$ other subnets. Inter- and intrasubnet routing are supported by combining packet-rate wavelength conversion within the ONIR's with the passive wavelength routing function of an $N \times N$ WDM arrayed waveguide grating router (AWGR) [7]. Wavelength reuse is supported since multihop routing with wavelength conversion allows access to a large number of nodes using only N wavelengths.

Routing and packet forwarding functions that are supported by the ONIR's include wire rate header recovery and updating, fast wavelength switching, spatial optical switching, and packet forwarding processing. Header updating is an important function that can simplify network routing and support label swapping for future internet protocols and ATM switching. An important issue not addressed in detail here is that of optical contention resolution, which we discuss briefly in next section and has been studied by several groups [8], [9].

Manuscript received June 5, 1998. This work was supported by an NSF National Young Investigator Award 9457148 and a DARPA DURIP Award DAAH04-96-1-0346. The work of A. Carena and R. Gaudino was supported by a grant from AEI—Associazione Elettronica ed Elettrotecnica Italiana. The work of M. D. Vaughn was supported by Corning Incorporated, Corning, NY.

A. Carena and R. Gaudino are with the Dipartimento di Elettronica, Politecnico di Torino, Torino, Italy.

M. D. Vaughn is with the Optical Communications Research Department, Corning Incorporated, Corning, NY 14831 USA.

M. Shell was with the Department of Electrical and Computer Engineering, Optical Communications and Photonic Networks Laboratory, University of California, Santa Barbara, CA 93106 USA. He is now with the Department of Electrical and Computer Engineering, Georgia Institute of Technology, Atlanta, GA 30332 USA.

D. J. Blumenthal is with the Department of Electrical and Computer Engineering, Optical Communications and Photonic Networks Laboratory, University of California, Santa Barbara, CA 93106 USA.

Publisher Item Identifier S 0733-8724(98)09569-3.

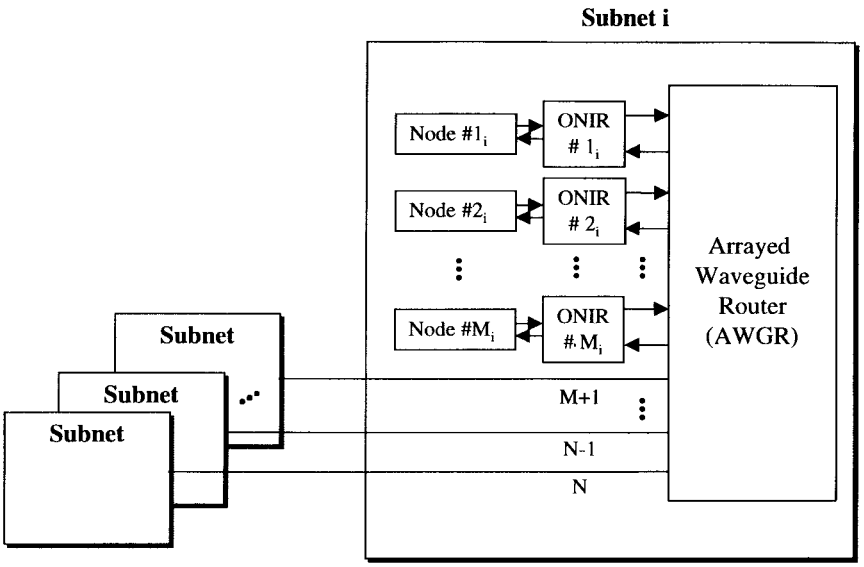

Fig. 1. OPERA network illustrating local connections within a subnet and connections between subnets. Routing, packet forwarding, and label swapping are performed using the optical network interface routers (OINR's) and arrayed waveguide routers (AWGR's).

OPERA uses an optical subcarrier multiplexed (OSCM) addressing format [10], [8], [11] to simplify packet header recovery and updating. The payload and header are transmitted at different bit rates and header recovery is performed independent of the payload data rate using simple microwave filtering techniques. Subcarrier header recovery is performed using optical and microwave direct detection alleviating the need for RF coherent techniques and phase synchronization across the network. Wavelength conversion is performed at the packet rate and a novel two stage wavelength conversion approach supports optical subcarrier replacement and payload extinction ratio enhancement. This approach is based on semiconductor optical amplifier wavelength converters and provides optical header removal without detection of the payload and header replacement using narrowband electronics. Node-by-node optical 2R payload regeneration and OSCM header replacement implements a router that is cascadable over multiple hops and that overcomes dispersion limitations to double sideband subcarrier multiplexing up to a 30 km internode distance.

III. Packet Coding and Addressing

An important issue in optical packet switched networks is packet coding and addressing. The information required to route and/or control the packet is usually encoded in a digital preamble that travels together with the payload. The approach of attaching a header to the beginning of a packet in the same format used for the payload requires routing nodes to process the full payload bandwidth to make a routing decision.

Several groups have demonstrated encoding of header information on a subcarrier signal modulated over the same optical wavelength used for the baseband signal [10], [8], [9], [12]. Using this OSCM technique, the header is encoded using a much lower bit rate than the payload rate. Recovery of the header is asynchronous to the high data rate payload and can be easily detected by a photodiode followed by microwave bandpass filters without knowledge of the payload timing. Using square law microwave detection, phase insensitive header recovery simplifies the node and network architecture relative to coherent techniques. Additionally, using a SCM header addressing technique lends itself to a new optical RF signal processing technique that suppresses the SCM header while wavelength converting the payload and finally remodulation of a new header. The routing node electronics therefore only needs to operate over the narrow electronic bandwidth of the header channel.

The OSCM packet addressing technique is shown in Fig. 2 and is described in more detail in [13]. A differentially modulated interferometric modulator is used to impress baseband payload and subcarrier multiplexed header data onto an optical carrier. The RF power spectrum of the packet is shown in Fig. 2. A novel modification of this approach is applied to label swapping and payload regeneration by combining header replacement and payload wavelength conversion in an interferometric structure as described in the next section.

A primary issue with fiber propagation of double sideband (DSB) OSCM is related to chromatic dispersion. The subcarrier signal can be completely attenuated due to deep notches present in the fiber RF frequency transfer function. As an example, when $f_{\text{subcarrier}} = 10$ GHz and a dispersion shifted fiber is used ($|D| < 1.5$ [ps/nm/km], the first notch is reached when L is approximately 100 km. Therefore, DSB-OSCM is impractical for high subcarrier frequencies over long end-to-end distances. While this issue has been addressed using single sideband modulation for fiber links in RF photonics [14], [15], there has been little attention paid to application to optical networks.

In the OPERA architecture, one of the intrinsic advantages is the use of a subcarrier replacement technique on a node-by-node basis. Since the subcarrier signal is optically regenerated at each node, it sees only the dispersion accumulated on a node-to-node distance rather than on the end-to-end distance.

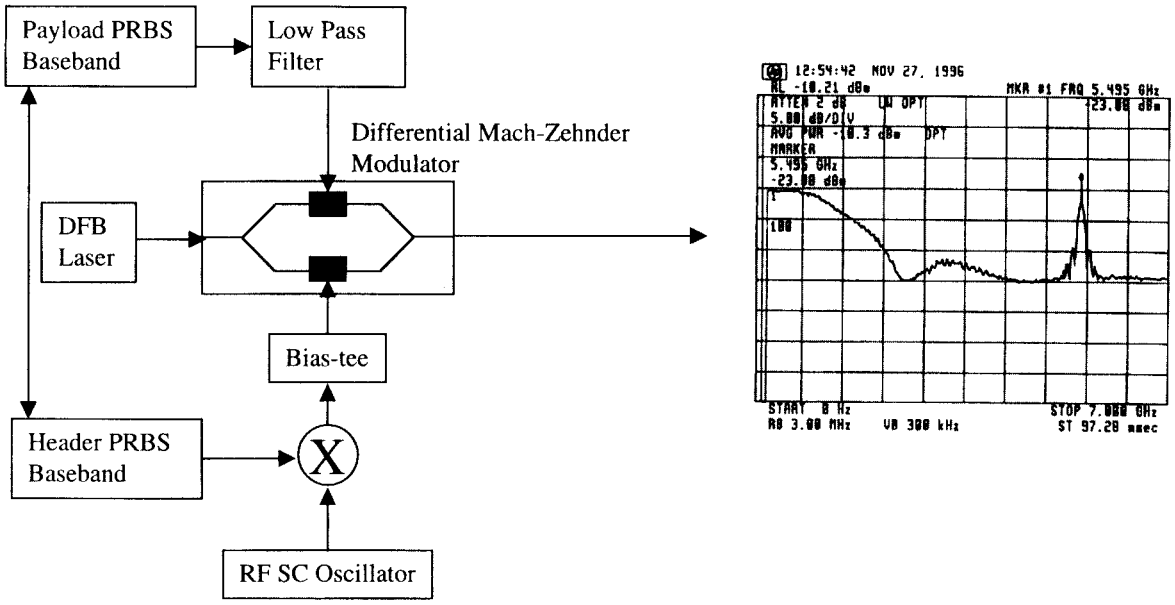

Fig. 2. Differential interferometric transmitter used to generate packets with payload at baseband and header multiplexed on a subcarrier. Also shown is resulting RF power spectrum.

The advantages of this approach are shown through time domain simulations presented in the next section. The capability to support DSB-OSCM reduces the transmitter and header receiver complexity.

IV. The Optical Network Interface Router

The ONIR handles routing and packet forwarding operations between the local host and two ports of the local AWGR. Packets entering the ONIR are processed and either dropped to the local host or wavelength converted with header updating and payload regeneration and forwarded to the AWGR for routing at the next ONIR. Packets to be transmitted from the local host are stored in a queue within the ONIR and added to the network when the output link is available.

A functional description of the ONIR is shown in Fig. 3. Depending on the network load and traffic distribution, there is a finite probability that temporally overlapping WDM packets can enter the ONIR. Since the basic ONIR processes one packet at a time, an optical contention resolution circuit similar to that reported in [8], [9] is required. A portion of the packet's optical power is tapped and photodetected for header recovery using a burst mode receiver that enables fast header recovery through adaptive thresholding and fast clock acquisition [16]. Optical direct detection and microwave direct detection circuits are employed to recover double sideband subcarrier multiplexed headers [11].

For most packet switched applications, the recovered header contains either a destination address or virtual circuit (VC) number. The address or VC are input to a routing control processor with the current node ID to establish the new node state. The new node state specifies the setting of a local optical gates (G_l, a remote optical gate G_r), a new optical wavelength λ_{new} and a new subcarrier multiplexed header. In the absence of through-going packets, the routing control processor transmits queued packets from the local user.

The input packet is passed through a wavelength conversion stage that simultaneuously removes the OSCM header and converts the payload to an internal ONIR wavelength (λ_{int}) [4]. An optical fiber delay is used to match the node state computation and setup time with the propagation delay within the ONIR. When the packet address/VC and local I.D. match, the local optical gate G_l is opened while the remote optical gate G_r is closed. If the packet address does not match the local node I.D., the new wavelength and header are computed, G_l is closed, the payload is optically wavelength converted, a new subcarrier multiplexed header is modulated onto the outgoing packet and the gate G_r is opened. G_r is open only during the duration the packet is output to the AWGR. Output gating is required in order to prevent unwanted optical amplifier noise and laser power from entering the network.

A more detailed layout of the ONIR is shown in Fig. 4. This layout also shows an alternate approach to dropping and fowarding packets. In this case, the packets are optically regenerated prior to gating to the local host and may result in an improved payload SNR and increase in number of allowed hops. Wavelength conversion using cross-gain modulation (XGM) in a semiconductor optical amplifier wavelength converter (SOA-WC) provides high speed conversion of the payload to an internal wavelength (λ_{int}) while simultaneously suppressing the SCM header [4]. Fast, uniform wavelength conversion switching time is performed using a novel predistortion current injection circuit [17] in combination with a four-section wavelength tunable GCSR laser [18] yielding wavelength switching times under 10 ns, independent of source and destination wavelength.

Conversion to a single internal wavelength simplifies the local host receiver and requirements on interferometric optical modulators used at the node input and output. The output SOA-WC is an interferometric cross-phase modulation (XPM) SOA-WC that converts outgoing packets to the new wavelength.

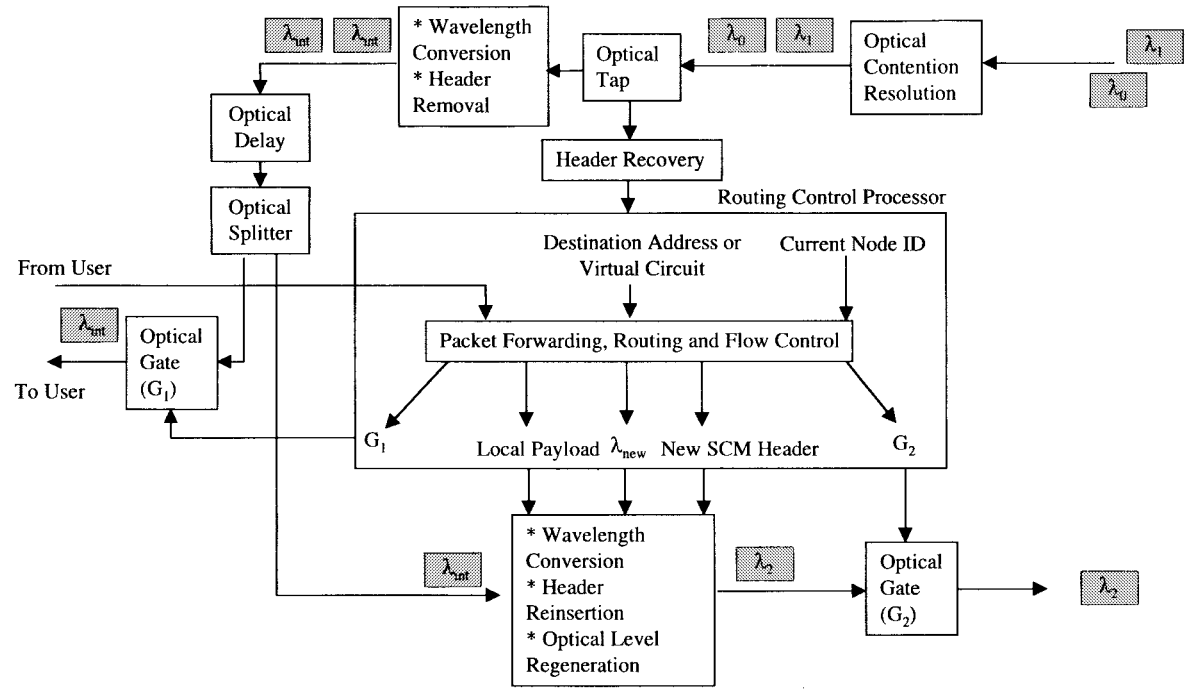

Fig. 3. Functional description of the ONIR.

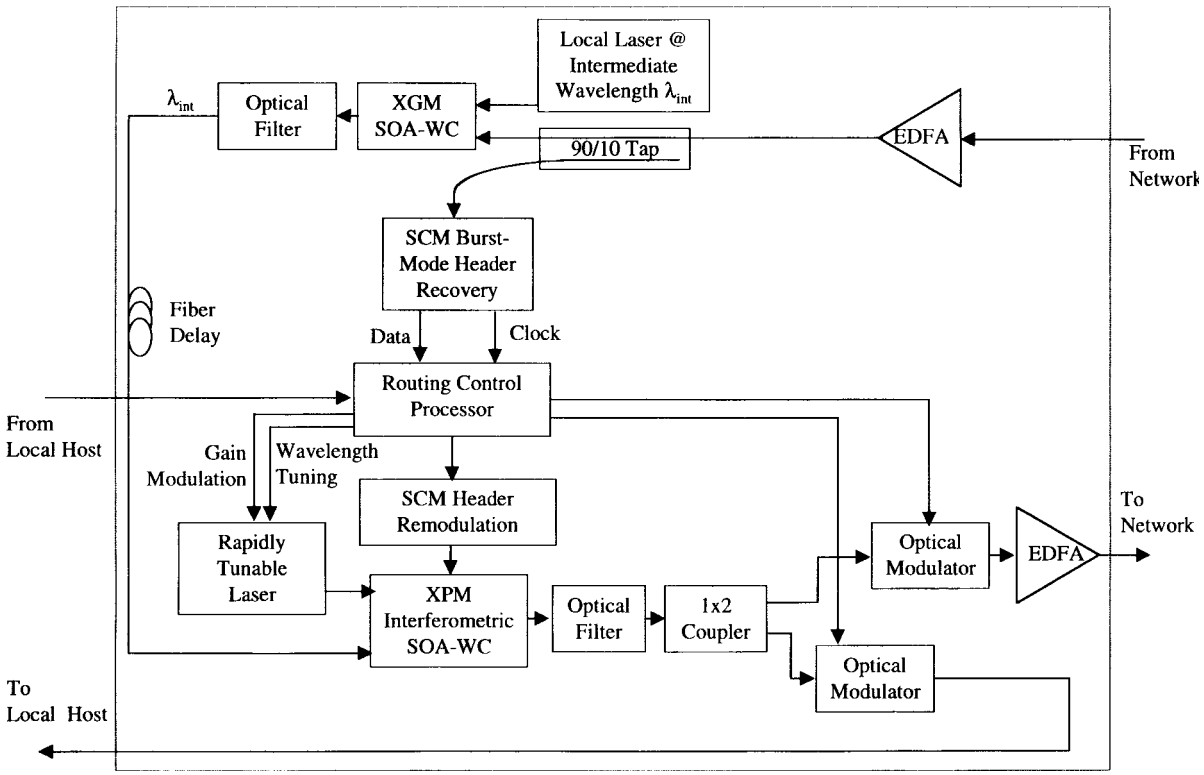

Fig. 4. Device-level layout of ONIR.

The cascaded wavelength converter with header replacement is shown in more detail in Fig. 5. The first XGM SOA-WC performs several functions including bit inversion, conversion to an internal wavelength, suppression of the SCM header, and reduction in modulation dynamic range. Conversion to an internal wavelength allows use of a fixed frequency optical filter to separate unconverted and converted signals and converter operating parameters to be optimized for only up- or down-wavelength conversion. While the payload is converted to a new wavelength via XGM, the SCM header is suppressed due to the low pass filter characteristics of the SOA-WC [4]. Reduction in output dynamic range of the first converter sets a stable operating point for the XPM interferometric SOA-WC [19]. The throughgoing payload and a new header

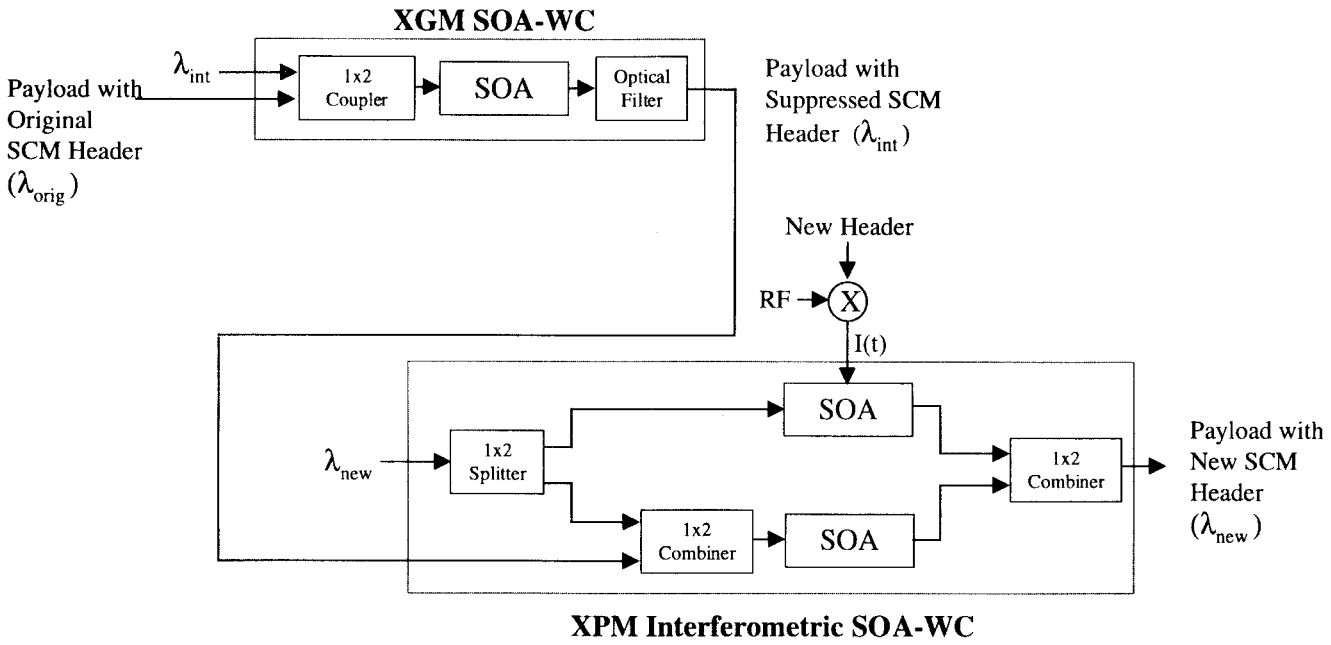

Fig. 5. Double stage SOA-based wavelength converter capable of optical header label swapping by subcarrier suppression and replacement. The first stage is based on XGM and the second on XPM interferometric structure. Subcarrier header replacement is performed with electronic modulation of SOA current in one arm of the interferometer.

are reassembled onto the new wavelength using an optical interferometric XPM SOA-WC configured in an analogous manner to the baseband/SCM transmitter reported in [13]. The XPM SOA-WC is operated in the inverting mode to negate inversion of the baseband in the XGM SOA-WC. Square law detection of the subcarrier makes header recovery insensitive to wavelength conversion inversion. The converted payload from the XGM SOA-WC is used to optically modulated the SOA in one arm of the interferometer to impress the payload onto ($\lambda_{\rm new}$). Current modulation of the SOA in the other arm is used to add a new SCM header onto the converted payload. The nonlinear transfer function of the XPM converter enhances the extinction ratio of the outgoing payload. Optical 2R regeneration of the payload combined with regeneration of the SCM header results in a cascadable packet switched node with label swapping capabilities.

V. Multihop Discrete-Time Physical Transport Simulation

Multihop packet propagation in OPERA was simulated using *OptSim*, a commercial discrete-time simulator [20] with custom functional blocks for SOA based wavelength converters and subcarrier transmitters and receivers developed for this research. The simulator performs linear (dispersion) and nonlinear (Kerr effect) fiber propagation calculations and takes into account the effects of EDFA ASE amplifier noise, optical filters, photodetection and photoreceiver noise. We use pseudo-random bit sequences (PRBS's) of repeat length 2^7-1 for the baseband and header. The simulator output for this work is in the form of eye diagrams. The computation is too intensive to simulate accurate bit error rate (BER) and Q values are not an accurate performance measure due to asymmetry in the eye diagrams and eye degradation due to baseband/subcarrier interaction within optical elements.

Simulation of the XGM and XPM SOA-WC's is based on an SOA model developed in [19] that treats the SOA as N cascaded sections, each one governed by a unique carrier density rate equation. A fourth-order Runge–Kutta algorithm was used to solve the carrier differential equation for each section. We then calculate the time varying material gain, index of refraction and change in phase delay for both signals within a single amplifier for each section. For the XGM SOA-WC, we propagate both the modulated original wavelength and a continuous wave (CW) local wavelength through the amplifier and recover the discrete time output of the converted signal. For the XPM interferometric SOA-WC, we considered a Mach–Zehnder interferometer (MZI) with SOA's in each arm, simulated as described above to recover the optical gain, index and phase. One SOA is optically modulated with the converted output of the XGM SOA-WC and the other SOA is current modulated with local SCM header. Both amplifiers also have a CW new wavelength coinjected from the first y-branch of the interferometer as shown in Fig. 5. We used SOA parameters listed in [21] with $N = 50$ sections for each SOA. This number of sections was choosen based on simulations that show convergence of the small signal frequency reponse.

A. Simulation Description

An initial SCM packet transmitter was modeled based on the architecture described in [13] and used to generate a 2.5 Gb/s baseband and a 100 Mb/s header ASK modulated onto a 15 GHz RF subcarrier. The average high and low modulated optical power levels for the combined local and modulated signals were balanced at the SOA-WC inputs and outputs to set the operating points for the baseband frequency response and extinction ratio at the ONIR output. The local laser power for the XGM SOA-WC was 5 mW and the local laser power for the XPM SOA-WC was 0.5 mW. These operating points

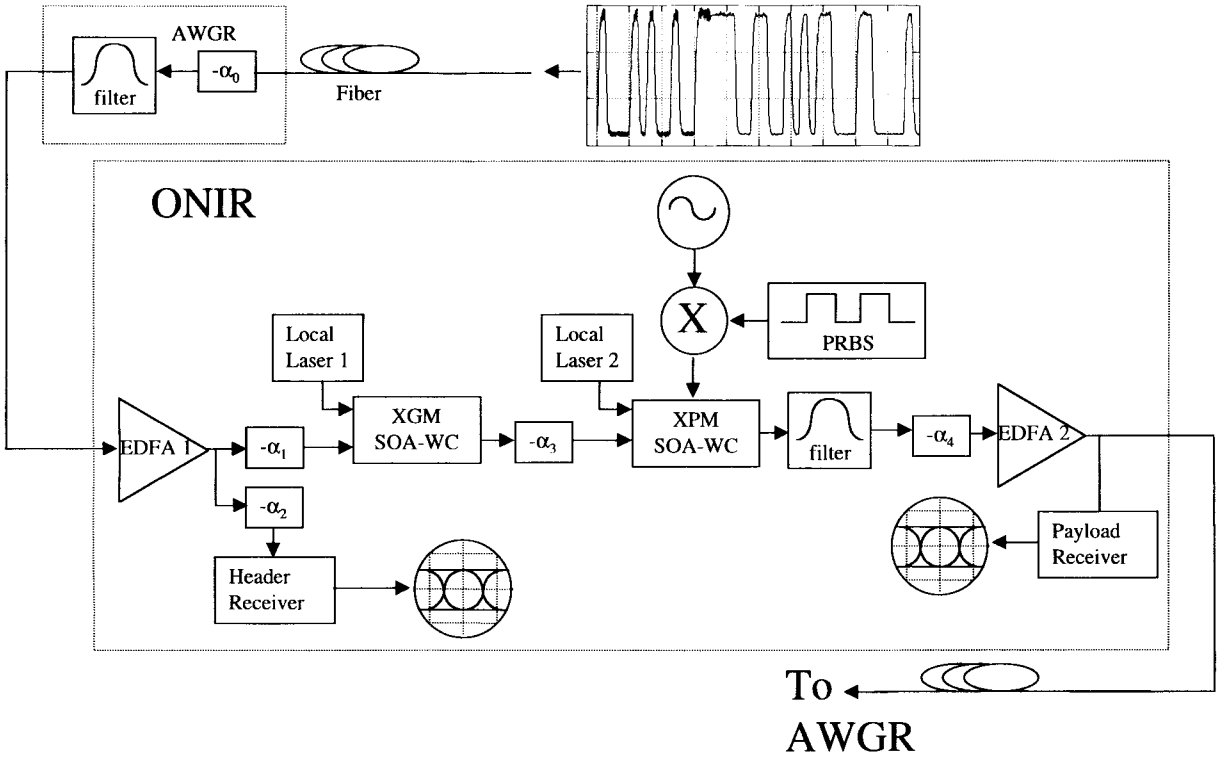

Fig. 6. Block diagram of fiber link, AWGR and ONIR models used in discrete time simulation. Signal inset shows payload bits with subcarrier modulated header bits. Multihop simulation was performed by cascading this basic element.

TABLE I
OPTICAL POWER LEVELS AND WAVELENGTHS AT DIFFERENT STAGES OF THE WAVELENGTH CONVERTER AS A FUNCTION OF HOP NUMBER

		NIU Input	XGM output	NIU output
$< P_{high} >$	[mW]	.47	27.0	.38
$< P_{low} >$	[mW]	.04	12.4	.03
λ_{hop1}	[nm]	1550.0	1510.	1553.2
λ_{hop2}	[nm]	1553.2	1510.	1556.4
λ_{hop3}	[nm]	1556.4	1510.	1543.6
λ_{hop4}	[nm]	1543.6	1510.	1546.8
λ_{hop5}	[nm]	1546.8	1510.	1553.2
λ_{hop6}	[nm]	1553.2	1510.	1540.4
λ_{hop7}	[nm]	1540.4	1510.	1556.4
λ_{hop8}	[nm]	1556.4	1510.	1550.0

TABLE II
GENERAL PARAMETERS USED IN DISCRETE TIME SIMULATION

Parameter	Value	Units
Subcarrier Frequency	15	[GHz]
Payload Bit-Rate	2.5	Gbit/s
Header Bit-Rate	100	Mbit/s
Internode Distance	30	[km]
Fiber Dispersion @ 1550 [nm]	2.	[ps^2/km]
Zero Dispersion Wavelength	1568.75	[nm]
EDFAs Noise Figure	4.5	[dB]
EDFA#1 Gain	18.2	[dB]
EDFA#2 Gain	17.1	[dB]
α_0	10	[dB]
α_1	0.46	[dB]
α_2	10	[dB]
α_3	12.5	[dB]
α_4	8	[dB]

were chosen to allow cascaded routing of a 2.5 Gb/s payload traversing 8 hops.

Operation of eight cascaded ONIR's interconnected by 30 km fiber links and an AWGR was simulated as described in Fig. 6. Here a baseband/OSCM packet is input to the fiber link followed by the AWGR simulated by a loss element and optical filter element. The ONIR is simulated using the shown gain, loss, filter and SOA-WC elements.

Power levels at different points within the ONIR and wavelengths for each hop at the same points are shown in Table I. Other general simulation parameters are listed in Table II. The loss parameters α_i consider device insertion losses. The loss parameter α_3 includes an extra 6.5 dB equalization loss used to balance the cascaded wavelength converters in addition to a 3 dB loss per fiber coupling to the SOA.

B. Simulation Results

The discrete time simulation results are shown in Figs. 7 and 8. Fig. 7(a) shows the time domain input to an ONIR from a previous node (λ_{orig}), illustrating the baseband modulation and superimposed subcarrier modulation. Fig. 7(b) shows the wavelength converted output (λ_{int}) of the XGM SOA-WC illustrating supression of the subcarrier, inversion of the baseband bit pattern, reduction in the extinction ratio and increase in the average optical power. The reduction in extinction ratio for the XGM SOA-WC helps to reduce the dynamic range at the input to the XPM SOA-WC leading to improved overall performance [22] for a two stage converter. The converted output of the XPM SOA-WC (λ_{new}) is shown in Fig. 7(c)

and illustrates noninverted bit conversion after two stages (due to operation of the second conveter in the inverting mode), replacement of the subcarrier signal and enhancement of the payload extinction ratio. The reduction in subcarrier amplitude during a payload zero bit relative to a payload one bit is due to a change in the XPM SOA-WC power transfer function with different average input powers. Therefore, there is a trade off between the amount of subcarrier amplitude reduction and the improvement of the extinction ratio of the output payload signal.

The result of PRBS propagation over 8 hops is shown in Fig. 8. The left hand set of eye diagrams shows the recovered baseband signal after 2, 4, 6, and 8 hops. Due to the low pass frequency response of the wavelength converters, cascading effectively reduces the total bandwidth of the system causing a continous closure of the eye opening. The bandwidth of each converter is determined by the average input optical power to the SOA. We chose the local laser power to set this bandwidth for 8 hop operation. The recovered header eye diagrams are shown in the right hand side of Fig. 8. Due to header regeneration at each hop, the eye opening remains stable after each hop over 30 km link propagation. Therefore, correct placement of the decision threshold will result in low error header recovery. The noise in the header one level is a pattern dependent crosstalk due to asynchronous switching with respect to the header of the baseband within the XPM SOA-WC. During a header one bit, the baseband switches many time between zeros and ones, changing the amplitude of the subcarrier in the one level due to the above mentioned effect.

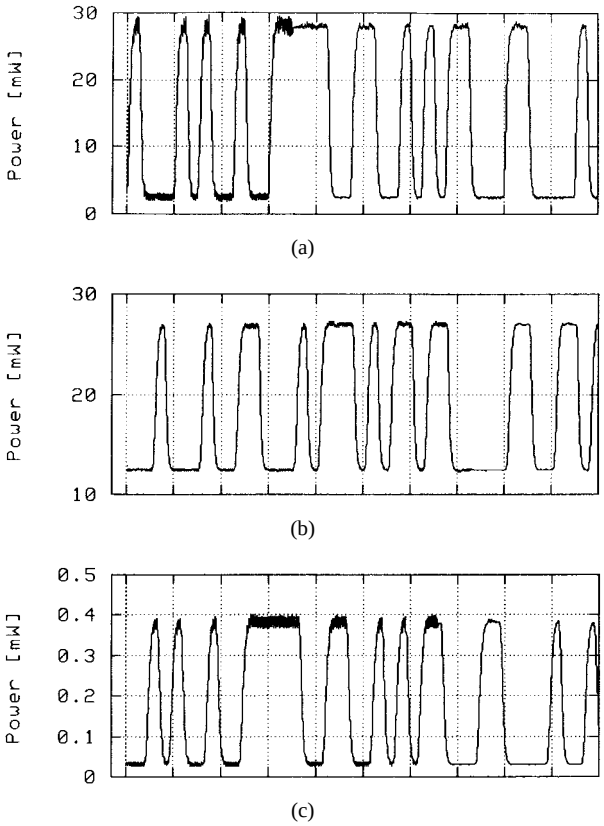

Fig. 7. Discrete time simulation results of baseband/oscm packets. Traces are for detected waveform in three different points of the ONIR: (a) input of the ONIR, after EDFA amplification, (b) output of first stage XGM SOA-WC, and (c) output of the ONIR, before EDFA amplification.

VI. Routing Experiments

A two node multihop experiment was constructed to demonstrate the basic ONIR operations of packet-rate wavelength conversion, header recovery and forwarding. In this multinode experiment, both payload and header were wavelength converted without replacement. Experimental demonstration of subcarrier header replacement using XGM SOA-WC's with 2.5 Gb/s baseband and 100 Mb/s header on a 16.5 GHz subcarrier was reported in [4].

The multinode experiment consists of a packet transmitter and two fully functional space/wavelength routing nodes interconnected by an 8×8 AWGR. Single stage packet-rate wavelength conversion by XGM in an SOA-WC without header replacement was used in this experiment. The packet transmitter generates packets of 1.22 μs duration with a 30 ns guard band at each end as described in [1]. Each packet consisted of a 3050-bit baseband payload at 2.5 Gb/s multiplexed with a 3.0-GHz subcarrier amplitude shift keyed (ASK) with a 100 Mb/s, 122 bit header. Header detection and recovery at each node were performed by tapping 10% of the input signal at the node input followed by optoelectronic conversion. Header recovery at node #2 was performed by using a microwave square law detector while header recovery at node #1 is performed by mixing the converted signal with a 3.0-GHz local oscillator (LO) followed by a 100-MHz low-pass filter. An ECL routing processor was used to map the recovered header and local node identification to one of two modulator states (local or remote) and one of four possible wavelengths (1538.1, 1552.0, 1561.8, and 1580.9 nm).

The four conversion wavelengths were obtained by changing the current in the coupler tuning section of a four-section tunable laser on a packet by packet basis as shown in Fig. 9. A novel predistortion pulse shaping circuit [17] is used to decrease the wavelength conversion times and reduce the variance across different source/destination wavelength pairs. In this multihop experiment, both payload and subcarrier multiplexed header were converted to the tunable laser wavelength via XGM in a SOA. $LiNbO_3$ interferometric optical modulators were used to gate packets to the local host or to the wavelength routed network.

Demonstration of packet routing through two nodes is shown in Fig. 10. The initial transmitter sends out a sequence of eight packets. Node #1 correctly identifies and routes the one packet that is destined for its local host. The other seven packets are correctly wavelength converted to one of four possible wavelengths based upon the recovered header bits of each packet. The wavelength converted packets are directed by the router to four different output ports based on packet wavelength. The reduction in signal strength of the 1581 nm packet is due to the fact that 1581 nm is outside the optimal wavelength range of the EDFA. Four packets are converted to 1538 nm and are routed to router output #1, which serves as the input to node #2. Node #2 then correctly handles these four packets. Two packets are recognized as being destined for

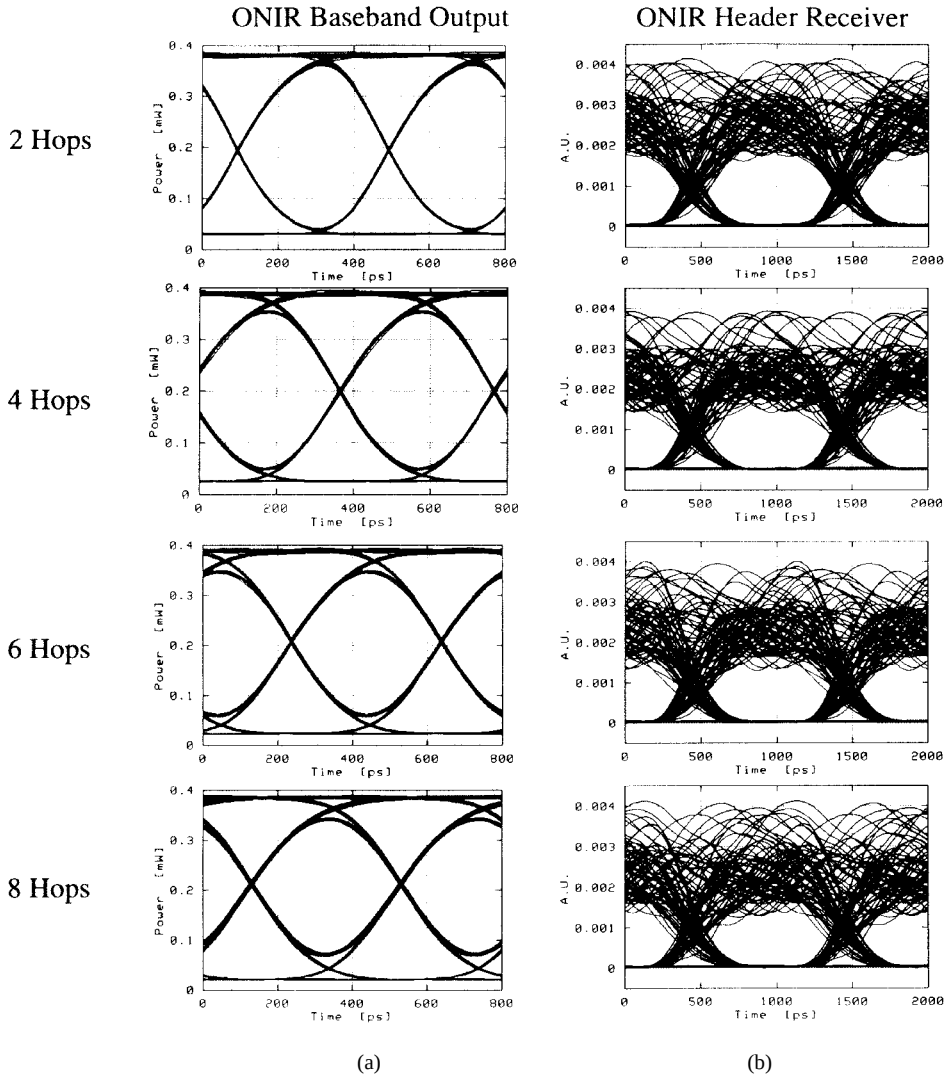

Fig. 8. Discrete time simulated eye diagrams showing cascadability of payload and header replacement after 8 all-optical hops. (a) is optical payload detected at the ONIR output after 2, 4, 6, and 8 hops. (b) is subcarrier header detected tapping off 10% optical power at ONIR input after 2, 4, 6, and 8 hops.

Node #2's local host. The other two packets are wavelength converted to two different wavelengths for further routing by the router.

Recovered eyes for the payload and the subcarrier control channels at the output of node #1 and at the output of node #2 are shown in Fig. 11(a) and (b), respectively. The Q values for all the eyes indicate bit error rate (BER) performance better than 10^{-9}. The reduction in the signal-to-noise ratio (SNR) of the recovered signals at node #2 is due to accumulated ASE noise from the EDFA's and SOA in the system as well as the loss in extinction ratio after the wavelength conversion process. The slower rise/fall times in the node #2 header are due to the fact that we chose a lower bandwidth header recovery filter at node #2 than at node #1. The recovered header signal at node #1 shows rise/fall times that are representative of the original transmitter output.

Experiments were also performed to demonstrate header removal and replacement using optical subcarriers and a XGM SOA-WC. The header was modulated on a 16.5 GHz subcarrier with a 2.5 Gb/s baseband as shown in Fig. 12(a). After wavelength conversion the header is suppressed significantly while the payload is transfered as shown in Fig. 12(b). The measured BER of the new header and wavelength converted payload as a function of old subcarrier header power for a XGM SOA-WC [4] is shown in Fig. 12(c). The power penalty due to interfering baseband signal in this configuration is shown to be around 2.5 dB. These results were obtained using an integrated optic modulator after the XGM SOA-WC and suffer the degradation due to lower extinction ratio enhancement and intermodulation distortion between the payload and header. It is expected based on the reported simulation results, that the second stage XPM SOA-WC will greatly enhance the extinction ratio of the converted payload.

VII. Summary

We have described the experimental and simulation results of the optical packet experimental routing architecture (OPERA) project. The architecture is based on packet routing using optical network interface routers (ONIR) and arrayed

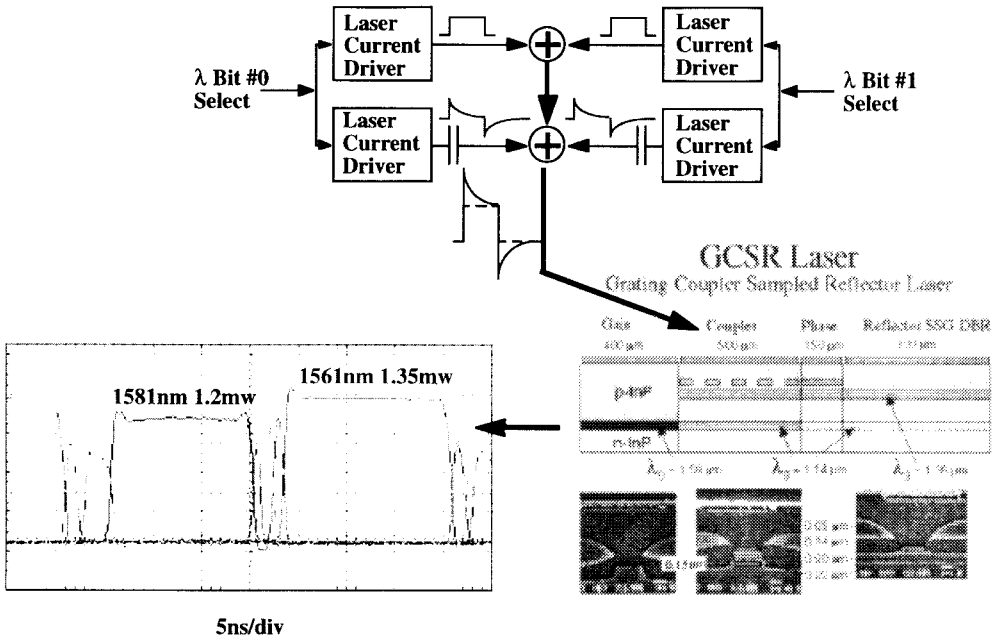

Fig. 9. Fast tunable GCSR laser with pulse predistortion circuit used for packet-rate wavelength conversion. Traces show wavelength switching times of 5 ns over 20 nm.

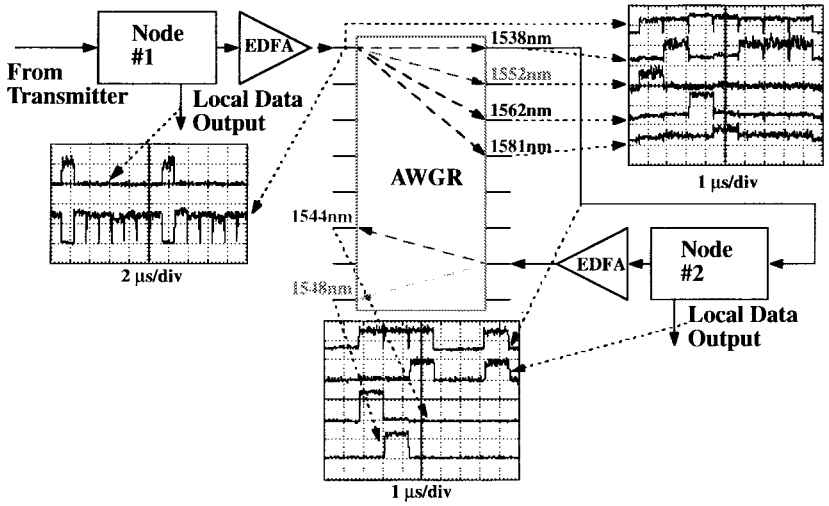

Fig. 10. Experimental demonstration of packet routing through two nodes and three passes through AWGR. Packets are header encoded and correctly dropped or forwarded with wavelength conversion.

waveguide router technology organized into subnets. The ONIR's are regenerative for both the payload and header and supports header updating, packet routing and forwarding operations and wavelength reuse. Header updating is an important function that can simplify network routing and support label swapping for future internet protocols and ATM switching.

The interface router incorporates a novel two stage SOA based wavelength converter design that supports optical removal and replacement of subcarrier headers supporting bit rate independent payloads out to the subcarrier frequency. The payload is 2R regenerated at each hop and the header is optically replaced at each hop. An 8 hop operation was evaluated using a discrete time simulator. The results show good performance for the payload with cascaded filtering effects causing eye closure with increasing number of hops. This eye closure can be managed by appropriate design of the local source power for the wavelength converter and power budget management of the links and nodes. The recovered header eye pattern at each ONIR shows complete regeneration on a hop by hop basis for double sideband subcarrier transmission. This result indicates that regeneration on a hop-by-hop basis with internode spacing on the order of 30 km allows the reduced complexity of double sideband transmission over that of single sideband transmission to be used.

Experimental demonstration of packet-rate wavelength conversion and packet forwarding based on SCM header recovery is described. Wavelength conversion was performed at the packet rate using a high-speed tunable laser with pulse predistortion circuit. Multihop routing was experimentally demonstrated between two all-optical nodes and three I/O ports

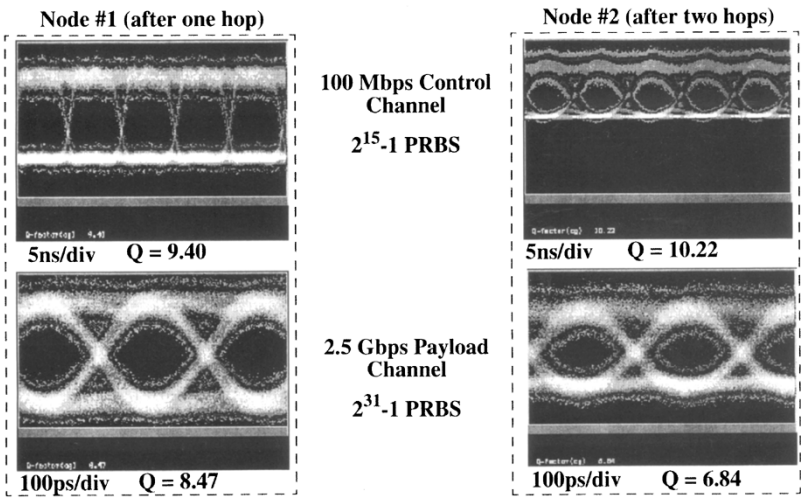

Fig. 11. Eye diagrams of the recovered payload and header channels for packets dropped at (a) node #1 and (b) node #2. The payload channel consists of a $2^{31} - 1$ PRBS pattern. The header channel consists of a $2^{15} - 1$ PRBS pattern.

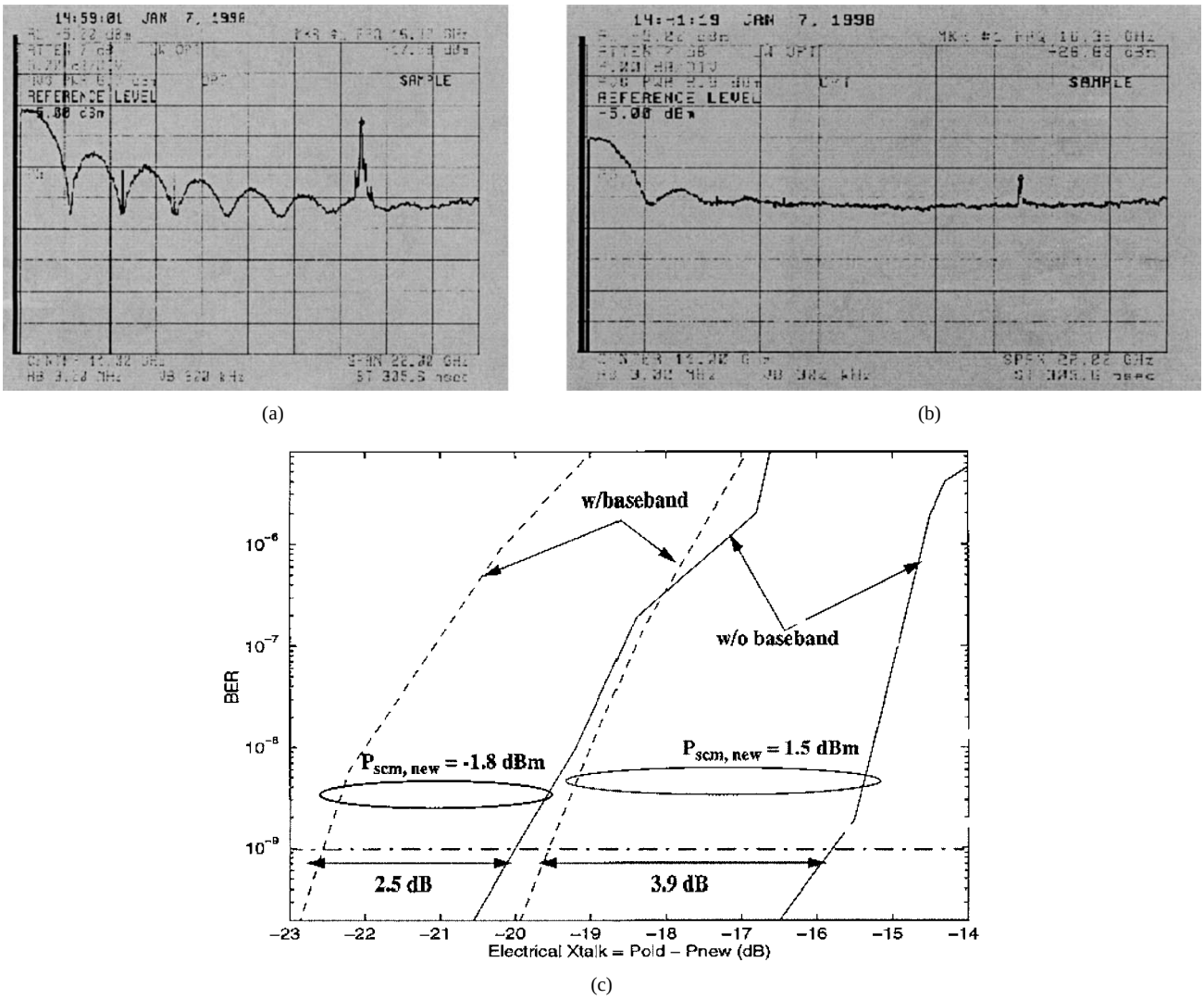

Fig. 12. Demonstration of header replacement using a XGM SOA-WC. (a) Input RF power spectrum, (b) wavelength converted power spectrum with suppressed subcarrier header, and (c) BER measurements of recovered baseband and new header in the presence of interfering unsuppressed old header.

of a waveguide grating array router. Packet-rate subcarrier header processing and wavelength conversion between six wavelengths is shown with high SNR of recovered payload and headers at each hop. Experimental results of optical header replacement using a cross-gain SOA based wavelength converter is also described showing that the payload and new header can be recovered with better than 10^{-9} BER.

Future work on OPERA includes incorporation of an experimental optical contention resolution circuit and cascaded XGM-XPM converter with subcarrier header removal and updating via current modulation of the output interferometer. Transmission loop testing of cascadability is also important to verify the reported simulation results. The feasability of single-sideband header techniques is also under investigation to extend the internode distances to beyond 30 km.

ACKNOWLEDGMENT

The authors wish to thank P. J. Rigole and S. Nilsson for the use of the GCSR tunable lasers and Artis s.r.l. for use of the Optsim simulator.

REFERENCES

[1] M. Shell, M. D. Vaughn, A. Wang, D. J. Blumenthal, P. J. Rigole, and S. Nilsson, "Experimental demonstration of an all-optical routing node for multihop wavelength routed networks," *IEEE Photon. Technol. Lett.*, Oct. 1996, pp. 1391–1393.

[2] E. Park and A. Willner, "Network demonstration of self-routing wavelength packets using an all-optical wavelength shifter and QPSK subcarrier routing control," in *Proc. Conf. Optical Fibers Commun.*, San Jose, CA, 1996.

[3] A. Viswanathan, N. Feldman, Z. Wang, and R. Callon, "Evolution of multiprotocol label switching," *IEEE Commun. Mag.*, vol. 36, pp. 165–173, May 1998.

[4] M. Vaughn and D. Blumenthal, "All-optical updating of subcarrier encoded packet headers with simultaneous wavelength conversion of baseband payload in semiconductor optical amplifiers," *IEEE Photon. Technol. Lett.*, vol. 9, pp. 827–829, June 1997.

[5] R. M. Fortenberry, Y. Cai, and R. S. Tucker, "Optically transparent nodes for photonic-switched ring networks," *Electron. Lett.*, vol. 29, pp. 417–418, 1993.

[6] K. S. Jepsen, A. T. Clausen, B. Mikkelsen, H. N. Poulson, and K. E. Stubkjaer, "All-optical network interface for bit synchronization and regeneration," in *Proc. European Conf. Optic. Commun.*, Edimburgh, UK, 1997.

[7] C. Dragone, "An $n \times n$ optical multiplexer using a planar arrangement of two star couplers," *IEEE Photon. Technol. Lett.*, pp. 812–815, Sept. 1991.

[8] C. L. Lu, D. J. M. Sabido, P. Poggiolini, R. T. Hofmeister, and L. G. Kazovsky, "CORD—A WDMA optical network: Subcarrier-based signaling and control scheme," *IEEE Photon. Technol. Lett.*, vol. 7, pp. 555–557, May 1995.

[9] K. Sasayama, Y. Yamada, K. Habara, and K. Yukimatsu, "FRONTIERNET: Frequency-routing-type time-division interconnection network," *J. Lightwave Technol.*, vol. 15, pp. 417–429, Mar. 1997.

[10] A. Budman, E. Eichen, J. Schlafer, R. Olshansky, and F. McAleavey, "Multigigabit optical packet switch for self-routing networks with subcarrier addressing," in *Proc. Conf. Optic. Fibers Commun.*, San Jose, CA, 1992, pp. 90–91.

[11] D. J. Blumenthal, J. Laskar, R. Gaudino, S. Han, M. D. Shell, and M. D. Vaughn, "Fiber-optic links supporting baseband data and subcarrier-multiplexed control channels and the impact of MMIC photonic/microwave interfaces," *IEEE Trans. Microwave Theory Tech., Special Issue on Microwave Photonics*, vol. 45, pp. 1443–1452, Aug. 1997.

[12] R. Gaudino, M. Shell, M. Len, G. Desa, and D. J. Blumenthal, "Mosaic: A multiwavelength optical subcarrier multiplexed controlled network," *IEEE J. Select. Areas Commun.*, vol. 16, pp. 1270–1285, Sept. 1998.

[13] R. Gaudino and D. J. Blumenthal, "A novel transmitter architecture for combined baseband data and subcarrier-multiplexed control links using differential Mach-Zehnder external modulators," *IEEE Photon. Technol. Lett.*, vol. 9, pp. 1397–1399, Oct. 1997.

[14] B. Davies and J. Conradi, "Hybrid modulator structure for subcarrier and harmonic subcarrier optical single sideband," *IEEE Photon. Technol. Lett.*, vol. 10, pp. 600–602, Apr. 1998.

[15] G. Smith, D. Novak, and Z. Ahmed, "Overcoming chromatic-dispersion effects in fiber-wireless systems incorporating external modulators," *IEEE Trans. Microwave Theory Tech.*, vol. 45, pp. 1410–1415, Aug. 1997.

[16] Y. Ota, R. Swartz, V. Archer, S. Korotky, M. Banu, and A. Dunlop, "High-speed, burst-mode, packet-capable optical receiver and instantaneous clock recovery for optical bus operation," *J. Lightwave Technol.*, vol. 12, pp. 325–331, Feb. 1994.

[17] P. J. Rigole, M. Shell, S. Nilsson, D. J. Blumenthal, and E. Berglind, "Fast wavelength witching in a widely tunable gcsr laser using a pulse pre-distortion technique," in *Proc. Optic. Fiber Commun. Conf. (OFC '97)*, 1997, pp. 231–232.

[18] P. J. Rigole, S. Nillsson, L. Backbom, T. Klinga, J. H. Walin, B. Stalnacke, E. Berglind, and B. Stoltz, "114 nm wavelength tuning rande of a vertical grating assisted codirectional coupler laser with a super structure grating distributed bragg reflector," *IEEE Photon. Technol. Lett.*, vol. 7, pp. 697–699, July 1995.

[19] T. Durhuus, B. Mikkelsen, and K. Stubkjaer, "Detailed dynamic model for semiconductor optical amplifiers and their crosstalk and intermodulation distortion," *J. Lightwave Technol.*, vol. 10, pp. 1056–1065, Aug. 1992.

[20] A. Carena, V. Curri, R. Gaudino, P. Poggiolini, and S. Benedetto, "A time-domain optical transmission system simulator package accounting for nonlinear and polarization-related effects in the fiber," *IEEE J. Select. Areas Commun.*, vol. 15, pp. 751–765, May 1997.

[21] M. D. Vaughn, *Optical Subcarrier Multiplexed Signal Processing Using Semiconductor Optical Amplifier*. Ph.D. dissertation, Georgia Inst. Technol., Atlanta, 1998.

[22] S. L. Danielsen, P. B. Hansen, K. E. Stubkjaer, M. Schilling, K. Wunstel, W. Idler, P. Doussiere, and F. Pommerau, "All optical wavelength conversion schemes for increased input power dynamic range," *IEEE Photon. Technol. Lett.*, vol. 10, pp. 60–62, Jan. 1998.

A. Carena, photograph and biography not available at the time of publication.

M. D. Vaughn, photograph and biography not available at the time of publication.

R. Gaudino, photograph and biography not available at the time of publication.

M. Shell, photograph and biography not available at the time of publication.

Daniel J. Blumenthal (S'91–M'93–SM'97), for a photograph and biography, see the Guest Editorial, p. 2066.